Journal of
Applied
Crystallography

ISSN 1600-5767

Received 25 October 2013
Accepted 17 March 2014

# Structural, electronic and magnetic properties of $YMnO_3/La_{0.7}Sr_{0.3}MnO_3$ heterostructures

**Amitesh Paul,[a]* Carlos Zandalazini,[b]‡ Pablo Esquinazi,[b] Carmine Autieri,[c] Biplab Sanyal,[c] Panagiotis Korelis[d] and Peter Böni[a]**

[a]Technische Universität München, Physik Department E21, Lehrstuhl für Neutronenstreuung, James-Franck-Strasse 1, D-85748 Garching bei München, Germany, [b]Division of Superconductivity and Magnetism, University of Leipzig, D-04103 Leipzig, Germany, [c]Department of Physics and Astronomy, Uppsala University, Box 516, SE-75120, Uppsala, Sweden, and [d]Laboratory for Neutron Scattering, Paul Scherrer Institut, CH-5232 Villigen, Switzerland. Correspondence e-mail: amitesh.paul@frm2.tum.de

Heterostructures with competing magnetic interactions are often exploited for their tailored new functionalities. Exchange bias is one such outcome of interfacial coupling across ferromagnetic–antiferromagnetic, multiferroic–ferromagnetic, two antiferromagnetic, or antiferromagnetic and paramagnetic interfaces. Apart from the usual horizontal shift of the hysteresis loop (exchange bias shift), a small 'vertical shift' of the hysteresis loops along the magnetization axis has also been seen, but it was always relatively small. Recently, an unusually large 'vertical shift' in epitaxial bilayer heterostructures comprising ferromagnetic $La_{0.7}Sr_{0.3}MnO_3$ and multiferroic orthorhombic $YMnO_3$ layers was reported. Here, using polarized neutron reflectometry, the magnetic proximity effect in such bilayers has been investigated. A detailed magnetic depth profile at the interface, elucidating the intrinsic nature of the vertical shift in such heterostructures, is reported. Further corroboration of this observation has been made by means of first-principles calculations, and the structural and electronic properties of $YMnO_3/La_{0.7}Sr_{0.3}MnO_3$ heterostructures are studied. Although in the bulk, the ground state of $YMnO_3$ is an *E*-type antiferromagnet, the $YMnO_3/La_{0.7}Sr_{0.3}MnO_3$ heterostructure stabilizes the ferromagnetic phase in $YMnO_3$ in the interface region. It is found that, in the hypothetical ferromagnetic phase of bulk $YMnO_3$, the polarization is suppressed, and owing to a large difference between the lattice constants in the *ab* plane a strong magnetocrystalline anisotropy is present. This anisotropy produces a high coercivity of the unusual ferromagnetic $YMnO_3$ phase at the interface, which is responsible for the large vertical shift observed in experiment.



## 1. Introduction

In perovskite-based heterostructures, magnetic interactions are particularly fascinating as they can show interface ferromagnetism between two antiferromagnets or between an antiferromagnet and a paramagnet (Ueda *et al.*, 1998). Competing magnetic interactions, which give rise to proximity coupling such as exchange bias, have found technological applications in magnetoresistive sensors. However, its microscopic origin often raises debate, particularly regarding the coupling configurations at the interface (Meiklejohn & Bean, 1956). Magnetic oxide heterostructures showing exchange bias have been reported earlier (Panagiotopoulos *et al.*, 1999; Moutis *et al.*, 2001; Ziese *et al.*, 2011, 2010). In oxide heterostructures, electronic and orbital reconstruction has received immense attention owing to its potential in relation to emerging novel electric and magnetic ground states. Combinations of ferroelectric (FE) and magnetic ordering in multiferroic oxides such as $TbMnO_3$ and $YMnO_3$, possessing noncollinear spin order, with collinear ferromagnets such as $La_{0.7}Sr_{0.3}MnO_3$, $La_{0.7}Ca_{0.3}MnO_3$ and Co have drawn considerable attention recently (Tian *et al.*, 2013; Barzola-Quiquia *et al.*, 2012; Zandalazini *et al.*, 2011).

Magnetic frustrations and noncollinear spin structures in the antiferromagnetic (AF) layer can often contribute to exchange bias in such functional thin-film heterostructures. Orthorhombic $YMnO_3$ (o-YMO) is ferroelectric as well. For hexagonal $YMnO_3$, $T_{FE} \simeq 900$ K and $T_N \simeq 80$ K, and for o-YMO, $T_{FE} \simeq 30$ K and $T_N \simeq 42$ K. It appears that ferroelectricity in hexagonal manganites is associated with a tilting

‡ Present address: Laboratorio de Física del Sólido, Universidad Nacional de Tucumán, 4000, Tucumán, Argentina.

of the Mn—O octahedra, whereas in o-YMO it has been proposed that it may result from the existence of a magnetic transition below $T_N \simeq 42$ K – from sinusoidal to helical spin order – that breaks the spatial inversion symmetry, thus allowing the existence of ferroelectricity. The Mn moments form an antiparallel spin order in the *ac* plane and can be characterized as a spin density wave with a helical angle propagating along the *b* axis. The propagation vector $\mathbf{k}_y$ subsequently experiences a magnetic reordering transition at some lower temperature (26 K) and locks into an incommensurate magnetic (ICM) structure (Munoz *et al.*, 2002). In this work, we focus on the coupling between FE o-YMO and ferromagnetic (FM) $La_{0.7}Sr_{0.3}MnO_3$ (LSMO).

Magnetic heterostructures showing a 'horizontal shift' of the hysteresis loop along the field axis have been commonly observed for conventional (Paul, 2012) as well as unconventional bilayer combinations (He *et al.*, 2012; Gibert *et al.*, 2012). However, an uncommonly observed effect of exchange coupling – across an AF–FM interface – is the shift along the magnetization axis or the 'vertical shift' (Hong *et al.*, 2006).

Element-specific magnetic studies with X-rays of $FeF_2$/Co and CoO/Fe (Ohldag *et al.*, 2003, 2006; Gruyters & Schmitz, 2008) layered structures confirmed the existence of this vertical shift and revealed its relation to specific uncompensated moments in the antiferromagnet. This vertical shift was often conjectured to be either correlated or not correlated to the bias field (Paul *et al.*, 2013). No convincing experiment could be carried out to possibly confirm this correlation owing to the extremely small magnitude of the vertical shift. Recently, a positive vertical shift in magnetization was shown to be related to the formation of an $Fe_3O_4$ ferrimagnetic interfacial layer (de la Venta *et al.*, 2012). Fitzsimmons *et al.* (2009) showed that only pinned spins within $DyFe_2$ would play a direct role in establishing the $m_{shift}$ (vertical shift) in hard–soft ferrimagnetic $DyFe_2/YFe_2$ layers. Noncollinear magnetic structure was predicted to be responsible for the vertical shift in an Fe/$MnO_2$ sample (Passamani *et al.*, 2006). Minor loop shifts are often mistaken as vertical shifts such as in the layered cobaltite (Geshev, 2008).

However, a recent study on heteroepitaxial interfaces involving $La_{0.7}Sr_{0.3}MnO_3/YMnO_3$ bilayers showed an unusually large vertical shift. It was also shown that this vertical shift was not correlated with the horizontal shift (Zandalazini *et al.*, 2011). Samples with a larger horizontal shift showed a smaller vertical shift and *vice versa*. In this paper, we establish that the ferromagnetic layer and the interdiffused layer between the AF–FM interface play a decisive role in determining the vertical shift of exchange-coupled heterostructural systems, which is strongly supported by our first-principles calculations. The paper is organized as follows. In §2, we discuss sample preparation and characterization. In §3, we show and discuss the experimental polarized neutron reflectivity results. In §4, we provide the first-principles calculations starting from bulk o-YMO and considering the structural, magnetic and electronic properties of the superlattices, and propose a microscopic mechanism to explain the large vertical shift. In §5, we present a summary and concluding remarks.

## 2. Samples and characterization

Bilayer heterostructures of [$La_{0.7}Sr_{0.3}MnO_3$ (80 Å)/$YMnO_3$ (3750 Å)] (LASMO) and [$La_{0.7}Sr_{0.3}MnO_3$ (300 Å)/$YMnO_3$ (3750 Å)] (LBSMO) were grown with pulsed laser deposition on 5 × 5 mm (100) $SrTiO_3$ (STO) substrates. The o-YMO layers were found to have orthorhombic structure. Details of the sample deposition and characterization are given by Zandalazini *et al.* (2011). The epitaxial nature of the growth was confirmed, along with the orthorhombic phase of the 3750 Å o-YMO layer. This layer presumably turns into an antiferromagnet or a dilute antiferromagnet in an external field (DAFF) at $T_N \simeq 42$ K, as outlined from the superconducting quantum interference measurements (SQUID) given by Zandalazini *et al.* (2011). However, the DAFF state disappears below 21 K (Okuyama *et al.*, 2011).

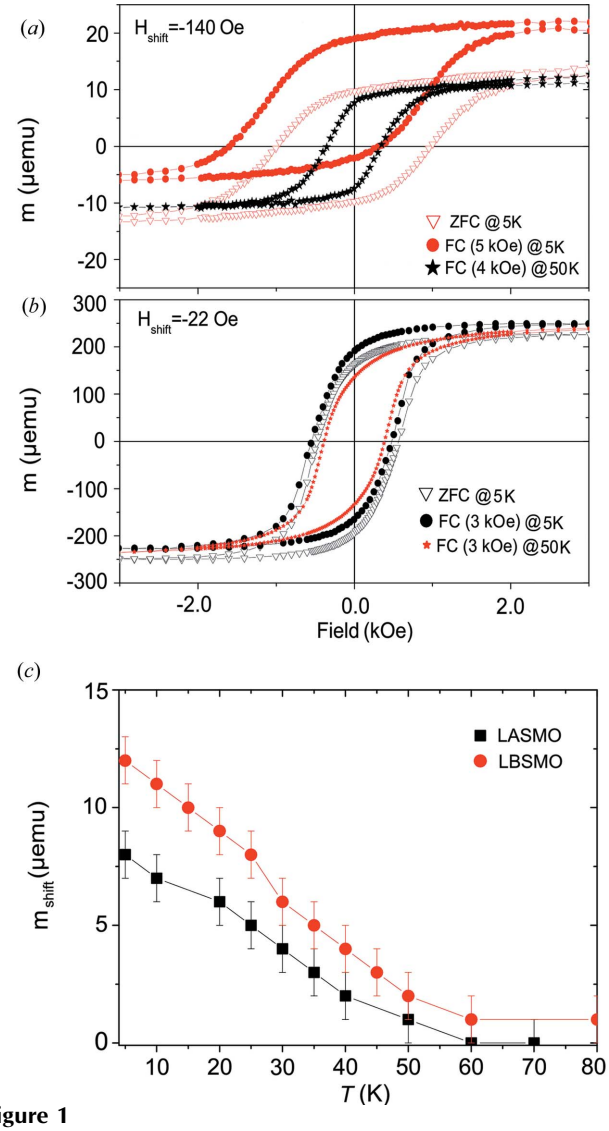


**Figure 1**
(*a*) LASMO and (*b*) LBSMO samples showing their respective exchange bias shifts and the vertical shifts [data from Zandalazini *et al.* (2011)]. (*c*) $m_{shift}$ *versus* temperature for the FC state at 4.0 kOe (LASMO) and at 3.0 kOe (LBSMO) without normalization with respect to the magnetic moment of o-YMO.

The temperature dependence of the remnant magnetization of the ferromagnetic LSMO layers showed a sudden change in slope close to the Nèel temperature of the underlying o-YMO layer (Zandalazini *et al.*, 2011). Field hysteresis measurements were made for the field-cooled (FC) and the zero-field-cooled (ZFC) cases as the samples were cooled from above $T_N$ down to 5 K. All the hysteresis loops showed the expected horizontal shift and also the 'vertical shifts' for both samples. The difference in the increase of the coercivities with lowering of temperature from 50 to 5 K indicates the different magnetic coupling at two different interfaces.

The horizontal shifts, defined by $H_{shift}$ [$= (H_c^+ + H_c^-)/2$, where $H_c^{+/-}$ are the coercive fields along the two branches of the loop], in the sample scale with the FM thickness (interfacial magnetic dilution with FM thickness). Note that the FM-layer thickness in the LASMO sample is around four times smaller than that in the LBSMO sample. However, the vertical shift [here we have defined the vertical shift as $m_{shift} = (m_s^+ + m_s^-)/2$] shows an anomaly as depicted in Figs. 1(*a*) and 1(*b*). The anomaly lies in the fact that the LASMO sample shows a larger $H_{shift}$ and a lower $m_{shift}$ as compared with a smaller $H_{shift}$ but larger $m_{shift}$ in the LBSMO sample. Fig. 1(*c*) shows the $m_{shift}$ without normalizing with respect to the magnetization of o-YMO. The LBSMO sample shows a 50% increase in $m_{shift}$ compared with the LASMO sample. Here $m_s^+$ and $m_s^-$ are the saturation moments along the two branches of the loops. This $m_{shift}$ was in surplus of any shift arising from the o-YMO magnetization (Zandalazini *et al.*, 2011). This became evident as the normalized $m_{shift}$ (normalized to the magnetization in the o-YMO layer measured separately) was shown to possess a larger value in LBSMO than in LASMO (increased from 7 to 13 μemu; 1 emu = $10^{-3}$ A m$^2$). This implies that the $m_{shift}$ in LASMO can be, to some extent, due to the o-YMO layer magnetization below 42 K. Therefore, the AF layer is not solely responsible for the observed $m_{shift}$ as o-YMO was deposited under similar conditions possessing the same thickness. Fig. 2 shows the ZFC and FC (0.5 kOe; 1 Oe = $10^3/4\pi$ A m$^{-1}$) measurements for the o-YMO and the LBSMO samples. The bifurcation of the FC and ZFC curves of o-YMO (3750 Å) gives the onset of the antiferromagnetic ordering temperature. The bifurcation of the ZFC and FC curves for LBSMO occurs at a much higher temperature, which is the blocking temperature ($T_B$ = 230 K) of the system. Following the initial report by Zandalazini *et al.* (2011), we felt the need to elucidate the intrinsic nature of the $m_{shift}$. We therefore used a depth-sensitive technique, namely polarized neutron reflectometry (PNR), to obtain the magnetic profile of the interface.

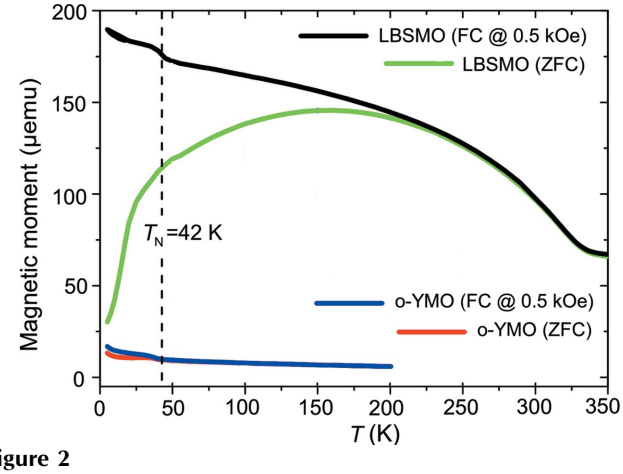


**Figure 2**
SQUID FC (at −0.5 kOe) and ZFC measurements for the o-YMO layer and that of LBSMO. The kink at $T_N$ in FC LBSMO shows that a ferromagnetic moment is created in the o-YMO.

PNR measurements were performed at the AMOR instrument at SINQ of PSI in Villigen (Switzerland). The data have been corrected for the imperfect polarization of the neutron beam. An in-plane magnetic field of −5 kOe was used to saturate the FM layer before the samples were cooled using a closed-cycle cryostat in the presence/absence of a field down to 50 and 10 K, respectively. The two temperatures were chosen so as to include (10 K) or exclude (50 K) the effect of enhanced o-YMO layer magnetization on the bilayer system. Note that the accessibility of the scattering vector ($\mathbf{Q}_z$) is limited, probably because of the buckling of the STO substrates below 104 and 64 K owing to structural transitions. Also note that the PNR data were measured at 50 and 10 K, which are below the buckling temperature of STO. Thus whatever changes one expects, as we compare the two data sets, would be independent of the buckling effect. It may be worth mentioning that the PNR measurements were technically extremely challenging given the small sizes (5 × 5 mm) of the samples. The magnetic field, perpendicular to the scattering plane, was produced with Helmholtz coils. The data treatment was carried out with in-house programs.

## 3. Polarized neutron scattering results and discussions

Owing to the comparatively large FE layer (3700 Å), an estimation of the individual FM-layer thickness was difficult from routine X-ray reflectivity (XRR) measurements. To get an estimate of the layer thicknesses, interface roughness, and nuclear ($\rho_n$) and saturation magnetic ($\rho_m$) scattering length density (SLD) values from the PNR data, the samples were measured at a saturation field of 5.0 kOe after cooling the samples down to 10 K in a cooling field of −5.0 kOe. Figs. 3(*a*) and 3(*d*) display our specular PNR data of LASMO and LBSMO bilayers.

The best fits (Figs. 3*a* and 3*d*, open symbols) with a simple model of block potentials yield average SLD values. One should note that PNR, unlike XRR, is highly sensitive to the magnetization of the layer stack irrespective of the thickness of the non-magnetic or antiferromagnetic layer at the bottom or at the top. The spin asymmetry (SA) in Figs. 3(*b*) and 3(*e*), expressed as the ratio of the difference and sum of spin-up and spin-down reflectivities, is also shown. The $\rho_m$ and $\rho_n$ depth profiles, obtained from the fitting, are shown in Figs. 3(*c*) and 3(*f*). The errors in the thickness of the LSMO (o-YMO) layers are ±2 nm (±100 nm), while those for the $\rho_n$ and $\rho_m$ values are $\pm 0.3 \times 10^{-6}$ Å$^{-2}$ ($\pm 0.5 \times 10^{-6}$ Å$^{-2}$) and $\pm 0.2 \times 10^{-6}$ Å$^{-2}$ ($\pm 0.2 \times 10^{-6}$ Å$^{-2}$), respectively.

The fits to the data were made considering the thickness of an interdiffused ($t_d$) layer at the interface of the LSMO and o-YMO layers. Note that, while it was necessary to consider the $t_d$ layer in the LBSMO sample, this layer was within the limit of the error bar for the LASMO sample. The errors in the thickness of the $t_d$ layer are ±20 Å, while those for the $\rho_n$ and $\rho_m$ values are $\pm 0.3 \times 10^{-6}$ Å$^{-2}$ and $\pm 0.2 \times 10^{-6}$ Å$^{-2}$, respectively. These values are used for the rest of the fits as the base parameters for different field cooling options and measuring fields. It may be also noted that the consistency of the analysis came from all available curves and a particular model was not considered from the fit of only one set of spin-up and spin-down curves.

Next we evaluate the data measured close to the remanence value after field cooling. Figs. 4(*a*)–4(*d*) show the specular PNR data on LASMO and LBSMO bilayers at 10 K and measured at 10 Oe. They compare the scattering intensities for the FC and ZFC cases. The average magnetization density in the bilayer is evident from the splitting of the spin-up and spin-down polarized curves measured at remanence. The best fits (open symbols) yield average SLD values. The $\rho_n$ and $\rho_m$ (at remanence) depth profiles, obtained from the fitting, are shown in Figs. 4(*e*)–4(*h*). SA is also shown in Figs. 5(*a*) and 5(*b*). The SA data clearly show the result of the splitting of the spin-up and spin-down polarized curves in both samples. The magnitude of SA in LASMO is much lower than in LBSMO.

Here, also, the best fit is obtained by considering an interdiffused layer of thickness $t_d$ at the interface of the LASMO bilayer. Next, we check the sensitivity of a magnetic interdiffused layer ($t_d$) at the o-YMO–LSMO interface on the profiles of the LASMO bilayer. We consider again a very small $t_d$ while the rest of the layers (SLD profile) remain the same as above. We show the effect for $t_d$ = 0, 20, 50 and 100 Å in Fig. 5(*c*). We note a deterioration of the overall fit quality beyond $t_d$ = 20 Å. However, when $t_d$ is below 20 Å, its effect becomes insensitive. No appreciable change was observed

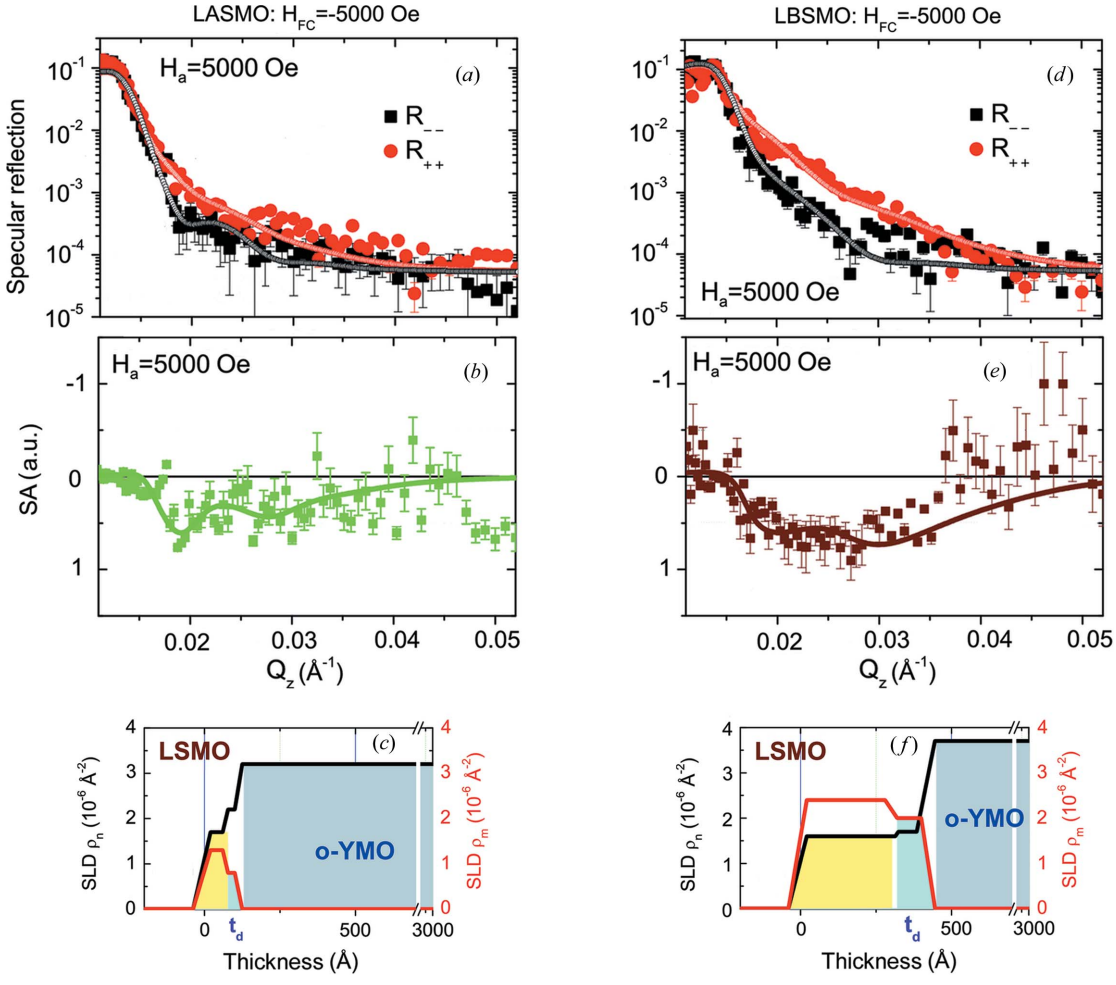


**Figure 3**
(*a*), (*d*) PNR curves at 10 K and at saturation (closed symbols) for spin-up and spin-down polarization of LSMO/o-YMO bilayers for the FC condition are plotted *versus* $\mathbf{Q}_z$ along with their best fits (open symbols) for samples LASMO and LBSMO, respectively. (*b*), (*e*) Spin asymmetry data, which are sensitive to magnetization, and their fits are plotted *versus* $\mathbf{Q}_z$. (*c*), (*f*) Depth profiles as obtained from fitting the data in (*a*) and (*d*) of the nuclear (black line) and magnetic (red line) scattering length densities, which are proportional to the nuclear and magnetic potentials, respectively. The slopes are indicative of their surface/interface roughnesses. The shaded regions in cyan show the interdiffused magnetic layers of 20 and 100 Å in their respective cases. Increasing height is the direction opposite to the growth direction.

(not shown) when the sample was measured at 50 K (the change in the magnetic moment from 10 to 50 K is only about 10 μemu).

From the fits of LASMO it follows that the $\rho_m$ of the 80 Å FM layer has increased from $1.0 \times 10^{-6}$ ($\pm$ 0.2) Å for the ZFC case to $1.5 \times 10^{-6}$ ($\pm$ 0.2) Å$^{-2}$ for the FC case, along with a change in sign of the magnetization. This sign change means that the net magnetization in the FC case is predominantly along the cooling field direction, whereas it is along the applied field ($\mathbf{H}_a$) direction for the ZFC case (as in the case of saturation). One may note that this remanent field magnetization that has been shown in the SQUID data was reached on coming from a positive saturation. The PNR data were collected directly after zero-field cooling. In this way, we maximize the possibility of a difference in the FM–AF exchange coupling as we expect to change the number of participating domains with cooling field. The loss in the net magnetization at remanence therefore stems from the randomness in the direction of the FM moments during the zero-field-cooling process.

The LBSMO bilayer, on the other hand, has developed an interdiffused layer at the FM–AF interface which has a thickness of ~100 Å. Moreover, this interdiffused layer possesses a magnetic SLD which is close to that of the FM layer. Comparison of the simulated data considering/not considering a magnetic interdiffused layer in the FC case is shown in Fig. 5(*d*). A difference in the deposition time for a thicker FM layer while holding the substrate temperature at 1073 K and depositing with the same frequency of repetition (10 Hz) of the laser pulse can plausibly be the cause of such an interdiffusion. In this sample, the net magnetization does not change its sign for the ZFC and FC cases, and always remains aligned along the direction opposite to the applied field. The change in $\rho_m$ for the FC with respect to the ZFC case is similarly increased by a small amount. The presence of an interdiffused magnetic layer would obviously result in an increase of the effective FM-layer thickness, which is primarily responsible for a significant decrease in the $H_{shift}$ in LBSMO.

The $\rho_n$ value of the $t_d$ = 100 Å layer has been found to be close to that of the LSMO layer. In order to verify the change

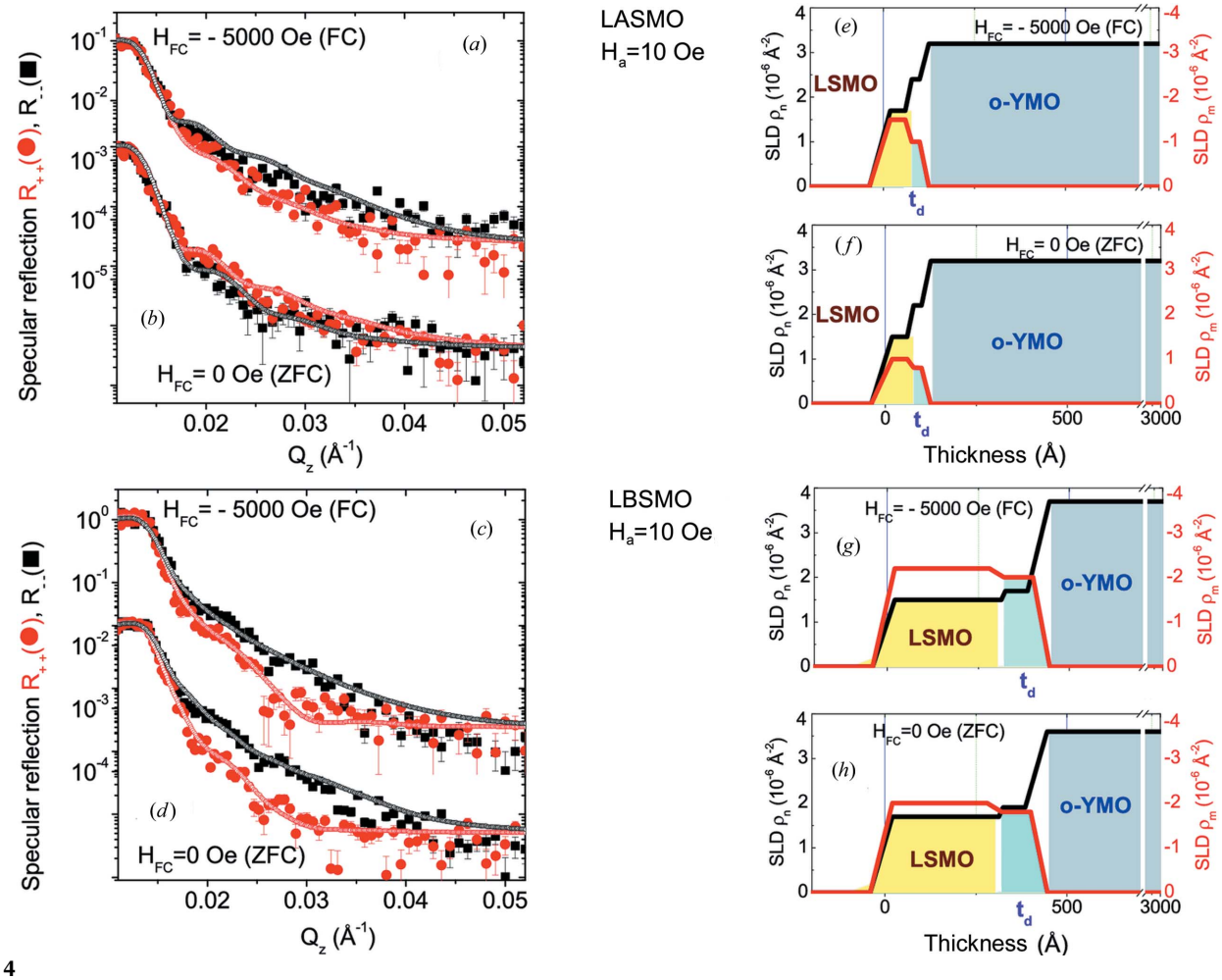


**Figure 4**
(*a*)–(*d*) PNR curves at 10 K and at remanence (closed symbols) for spin-up and spin-down polarization of LSMO/o-YMO bilayers for FC and ZFC conditions are plotted *versus* $\mathbf{Q}_z$ along with their best fits (open symbols). (*e*), (*f*) and (*g*), (*h*) Depth profiles as obtained from fitting the data in (*a*) and (*b*) of the nuclear (black line) and magnetic (red line) scattering length densities, which are proportional to the nuclear and magnetic potentials, respectively. The slopes are indicative of the surface/interface roughnesses. Note the positive $\rho_m$ in (*f*). The shaded regions in cyan show the interdiffused magnetic layers of 20 and 100 Å in the respective cases. Increasing height is the direction opposite to the growth direction.

in $\rho_n$ in LBSMO measured at 10 K, we show the effect of different $\rho_n$ values on the SA data in Fig. 6. A value close to that of the LSMO layer ($\rho_n = 1.5 \times 10^{-6}$ Å$^{-2}$) does not give the best fit. Thus the slight increase in $\rho_n$ (close to the limit of the error bar $\pm 0.3 \times 10^{-6}$ Å$^{-2}$) is justified.

Intuitively it appears that the large absolute $m_{shift}$ that we observe in the LBSMO bilayer is correlated with the interdiffused layer. In order to verify this, we measured the sample again in the ZFC and FC cases, but at 50 K (the changes in the magnetic moment from 10 to 50 K are about 40 µemu), as shown in Figs. 7(*a*)–7(*d*), along with the SA in Fig. 7(*e*). At 50 K, we expect neither a detectable vertical shift nor a horizontal shift ($T_N \simeq 42$ K).

From the fits to the data, to our surprise, we find that the thickness of the interdiffused magnetic layer is now significantly reduced (see the SLD profiles). Comparison of the simulated data considering/without considering a reduced magnetic interdiffused layer ($t_d \simeq 50$ Å) in the FC case is shown in Fig. 7(*f*). The $\rho_m$ values for the 300 Å FM layer on top of the o-YMO layer are somewhat lower than those estimated at 10 K in accordance with the earlier measurements (Zandalazini *et al.*, 2011), with no appreciable difference in their values for the FC and ZFC cases, as expected at this temperature. Thus the only significant difference in the SLD profiles, below and above $T_N$, is the effective thickness of the magnetic interdiffused layer.

Note that at 50 K we do not expect any vertical shift as the o-YMO layer is not AF anymore, whereas in LASMO the vertical shift still exists, even for a lower value of $t_d$, since the measurements are carried out at 10 K. A moment of $110 \times 10^{-6}$ emu at 50 K corresponds to around 0.9 $\mu_B$ per unit cell of LBSMO (ZFC), and at 10 K this gives a value around 0.5 $\mu_B$. The magnetic SLDs gives a comparable magnetic moment of 0.8 and 0.6 $\mu_B$ at 50 and 10 K, respectively.

A clear distinction between the existence of an interdiffused layer of $t_d = 20$ Å and its non-existence is difficult in the case of LASMO at 10 K (note the error bar in $t_d$ is also large at ±20 Å). In LBSMO, on the other hand, one can have a reasonable fit even with $t_d = 50$ Å at 50 K, which is a reduction from 100 Å at 10 K. However, the distinction is not clear from the FC data alone. In order to verify further the lowering of $t_d$, we show in Fig. 8(*a*) a similar comparison of the simulated data in the SA plot without considering/considering a reduced magnetic interdiffused layer in the ZFC case of LBSMO at 50 K. The effect of the thickness is clearer in this case as compared to the FC case. Also shown, in Fig. 8(*b*), is the effect of the magnetic $t_d = 50$ Å layer with different $\rho_m$ values. The reduction in $\rho_m$ is therefore also justified. Overall, the effective thickness of the magnetic interdiffused layer (which can be some combination of $t_d$ and $\rho_m$) is definitely lower at 50 K than at 10 K.

We note that the magnetization of the o-YMO layer may not be strictly be antiferromagnetic but rather diluted antiferromagnetic (developing domain states below $T_N$), which can lead to a net magnetization. The magnetism of the interdiffused layer can originate from the magnetism in the o-YMO

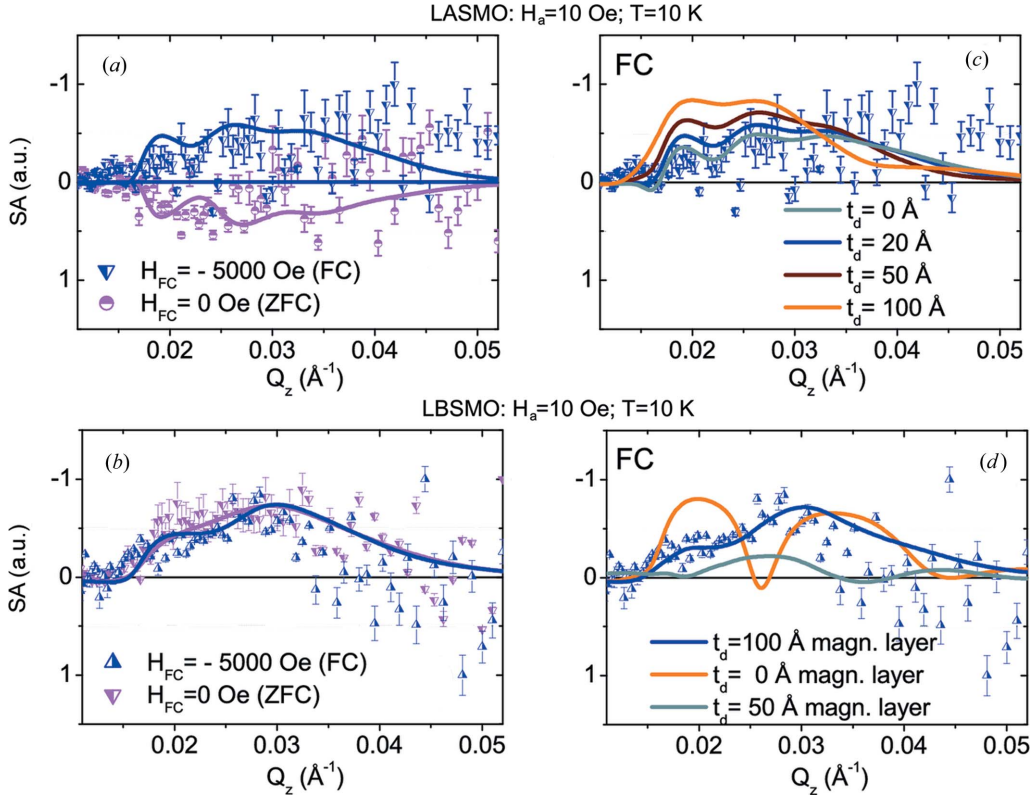


**Figure 5**
(*a*), (*b*) Spin asymmetry data, which are sensitive to magnetization, and their fits are plotted *versus* $\mathbf{Q}_z$. (*c*), (*d*) Comparison of the simulated data considering/not considering a magnetic interdiffused layer in the FC case. The effects of a small and a large magnetic interdiffused layer ($t_d$ = 0–100 Å) are also shown.

layer at the interface (Zandalazini *et al.*, 2011). Such a magnetism may turn antiferromagnetic depending upon the exchange coupling to the ferromagnet in its proximity. We note, however, that assuming reasonable values of the magnetization of a pinned interdiffused o-YMO layer (to account for the absolute value of $m_{shift}$), the thickness of this layer should have been much larger than the thickness we obtained here using PNR. In corroboration of the fact that the magnetism within the o-YMO layer reduces significantly above 50 K, and thereby the coupling with the LSMO layer, we find a significant reduction in the thickness of the magnetic interdiffused layer. At 50 K, this interdiffused layer will still be magnetic (to some extent) as the LSMO part of it will remain ferromagnetic and only the o-YMO layer will turn nonmagnetic. However, this magnetism is not extended over the entire o-YMO layer but is located at the o-YMO/LSMO interface only, as confirmed by model simulations of the data at 10 K (where the effect is most striking). The r.m.s. roughness at the LSMO/o-YMO interface estimated for LBSMO is around 75 (5) Å, whereas for LASMO it is around 35 (5) Å. Thus the observed interface magnetism is plausibly induced by the quality of interface structure and should be related to pinned moments at an FM interface due to stoichiometry variation of the LSMO layer.

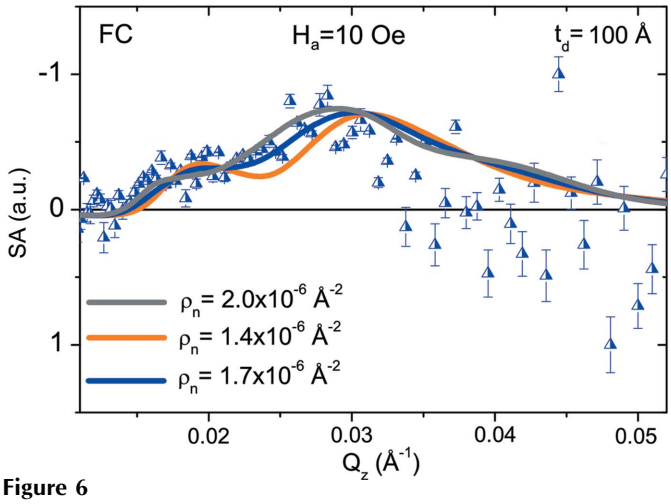


**Figure 6**
Spin asymmetry data, which are sensitive to magnetization, and their fits are plotted *versus* $\mathbf{Q}_z$ for LBSMO measured at 10 K in the FC case. Comparison of the simulated data considering a magnetic interdiffused layer ($t_d$ = 100 Å) with different values of $\rho_n$.

Exchange bias in LSMO/$BiFeO_3$ (Wu *et al.*, 2010) or LSMO/$TbMnO_3$ (Tian *et al.*, 2013) has also exhibited exchange coupling across FE–FM interfaces but without any reasonable vertical shifts. The unusually large vertical shift therefore

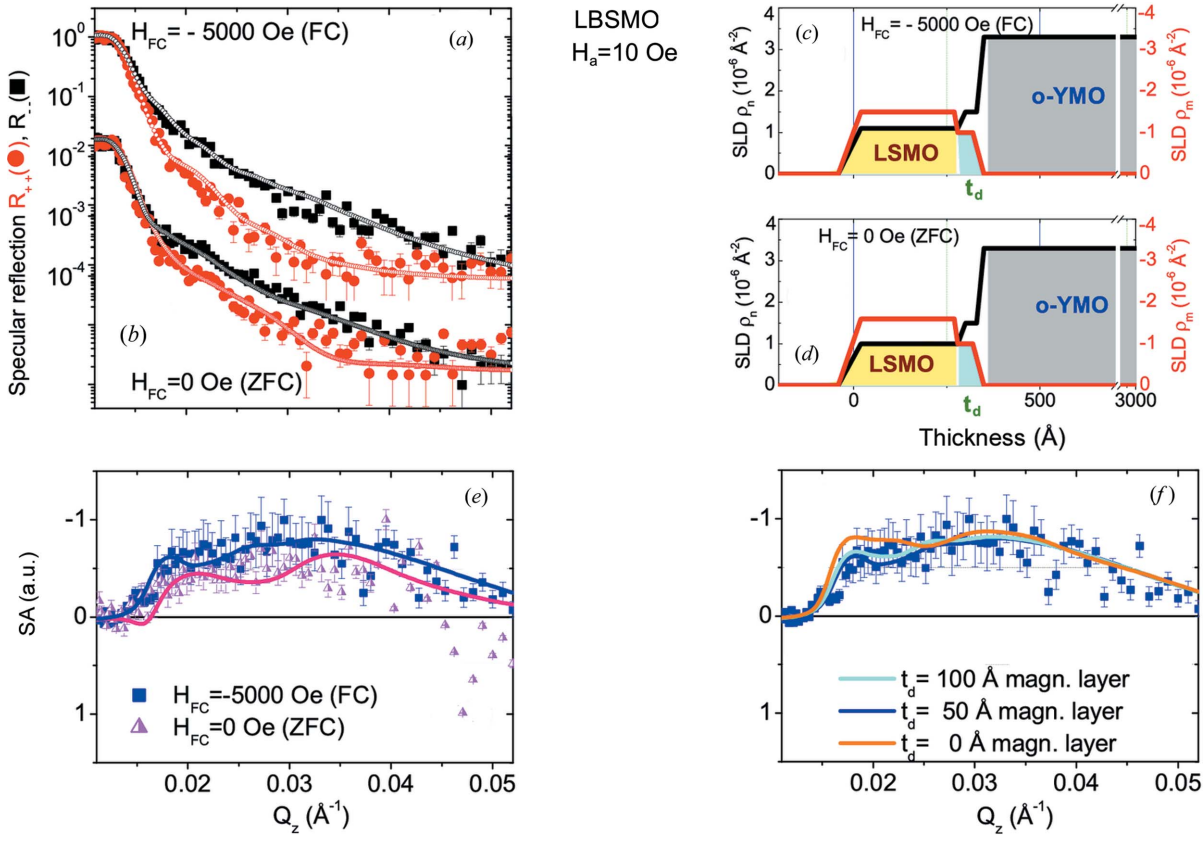


**Figure 7**
(*a*), (*b*) PNR curves at 50 K and at remanence (closed symbols) for spin-up and spin-down polarization of the LBSMO bilayer for FC and ZFC conditions are plotted *versus* $\mathbf{Q}_z$ along with their best fits (open symbols). (*c*), (*d*) Depth profiles as obtained from fitting the data in (*a*) and (*b*) of the nuclear (black line) and magnetic (red line) scattering length densities, which are proportional to the nuclear and magnetic potentials, respectively. The slopes are indicative of their surface/interface roughnesses. The shaded regions in cyan show the interdiffused magnetic layer of 40 Å. Increasing height is the direction opposite to the growth direction. (*e*) Spin asymmetry data, which are sensitive to magnetization, and their fits are plotted *versus* $\mathbf{Q}_z$. (*f*) Comparison of the simulated data considering/not considering a magnetic interdiffused layer in the FC case.

indicates the role of the magnetic interfacial coupling in our o-YMO-FM system. One may note that the large $m_{shift}$ that is observed here or in Co/o-YMO (Barzola-Quiquia *et al.*, 2012) is related to the influence of the o-YMO layer interface, whereas in Co/CoO the $m_{shift}$ is still observed but of much smaller magnitude (Zandalazini *et al.*, 2011). The noncollinear ICM spiral magnetic order that sets in for o-YMO at around 26 K may have important consequences for the proximity effect in these bilayers. Noncollinear magnetic order cannot be detected with the PNR technique as it probes the average FM component.

## 4. First-principles calculations

In order to elucidate the origin of the vertical shift which is correlated to the intermixed interface layer as inferred from the PNR data, we have performed first-principles density functional calculations by using the *VASP* package (Kresse & Furthmüller, 1996), based on a plane wave basis set and projector augmented wave method (Kresse & Joubert, 1999). For the treatment of exchange correlation, the Perdew–Burke–Ernzerhof (Perdew *et al.*, 1996) generalized gradient approximation has been considered. In order to include strong electron correlations, we have considered a Hubbard $U$ approach, commonly used to describe the electronic structures of correlated oxides. For the bulk parts of LSMO and o-YMO, we have considered $U$ values of 3 and 4 eV for the Mn $d$ orbitals, respectively, following the recommendations in the literature. As the appropriate value of the Coulomb parameter $U$ is unknown for the interface part, we have varied $U$ (1–5 eV) for interface Mn atoms and have examined the magnetic structures. In all calculations, the exchange parameter $J$ was kept as 0.7 eV. A $6 \times 4 \times 1$ $k$-points set was used for Brillouin-zone integrations in the Monkhorst–Pack scheme for the heterostructures. For bulk calculations, we have used a $6 \times 6 \times 6$ $k$-points mesh. The geometries were relaxed until the forces on all atoms were reduced to 5 meV Å$^{-1}$.

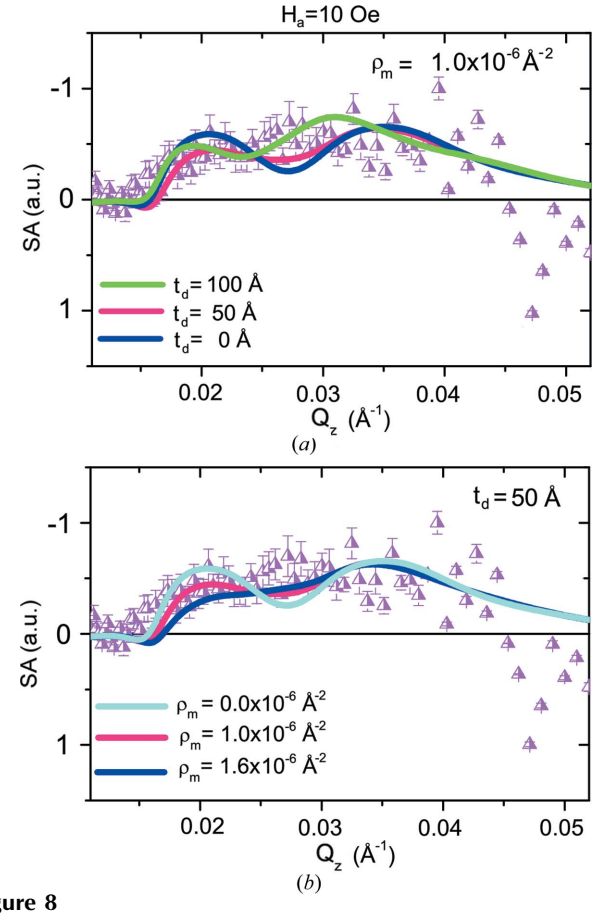


**Figure 8**
Spin asymmetry data, which are sensitive to magnetization, and their fits are plotted *versus* $\mathbf{Q}_z$ for LBSMO measured at 50 K in the ZFC case. Comparison of the simulated data considering (*a*) different thicknesses of magnetic interdiffused layer ($t_d$) and (*b*) different values of $\rho_m$.

### 4.1. Bulk $YMnO_3$

First, we have studied the properties of bulk o-YMO using the crystal structure provided by Okuyama *et al.* (2011) with lattice parameters $a$ = 5.246, $b$ = 5.830 and $c$ = 7.330 Å. It was shown that the charge on Mn atoms points towards the $b$ direction, creating a strong anisotropy between the two in-plane directions (Picozzi *et al.*, 2006). Depending upon the value of the Coulomb parameter $U$, we have three magnetic phases as the ground state: $E$-type, $A$-type and FM-type. Our results are in agreement with the results published by Picozzi *et al.* (2006). Our calculated polarization is along the $-\mathbf{a}$ direction, which is in agreement with the results in the literature (Okuyama *et al.*, 2011). The experimental value of polarization (Okuyama *et al.*, 2011) is between 0.25 and 0.5 μC cm$^{-2}$. However, in the FM phase, the electronic polarization is zero.

### 4.2. LSMO/o-YMO superlattices

Now we discuss the results for a heterostructure with two o-YMO layers, two LSMO layers and two interface layers. The layer between o-YMO and LSMO is named as the 'interface layer'. For simplicity, we have considered a sharp interface in this study. In our simulations, o-YMO is considered as the substrate for LSMO. We have used the experimental values of $YMnO_3$ for the in-plane lattice constants of the supercell (Okuyama *et al.*, 2011). For the initial structural model for the geometry optimization, the average out-of-plane separation between o-YMO and LSMO at the interface along the $c$ axis was considered. Relaxation of the atomic positions was performed for all the atoms including those at the interface until the forces acting on all the atoms became small.

In our interface model, we have a layer of YO, a layer of $MnO_2$ and another layer of LaSrO that closes the cage around the octahedra. However, the exact stoichiometry of the LaSrO layer at the interface is unknown. We have calculated the total energies for different magnetic phases and different Coulomb repulsion parameters and we find that the interface with only La atoms has always the lowest energy. Probably, the La atoms are energetically favored because of their atomic radii being very similar to the Y radii. Therefore, at the interface, we have the $MnO_6$ octahedra enclosed in a cage with Y on one side and

La on the other side. Because Y and La are electronically equivalent, there is no charge doping and hence the double exchange mechanism is not active at the interface. Thus the interface layer can be metallic or an insulator depending on the magnetic phase. On the other hand, the inner layers of LSMO will always be metallic because of the presence of Sr, which produces a charge doping. We find that the structural properties of the interface layer are intermediate between o-YMO and LSMO. For instance, the in-plane Mn—O—Mn bond angle is 148.0° for the interface layer, while it is 143.2° for o-YMO and 163.7° for LSMO for the fully ferromagnetic solution.

Here we discuss the most stable magnetic phases, but also *G*-type, *A*-type and *E*-type magnetic phases were studied at the interface. The three following magnetic phases are the most stable: (*a*) a fully ferromagnetic phase; (*b*) an antiferromagnetic *E*-type in o-YMO and a ferromagnetic phase in LSMO and the interface; (*c*) a ferromagnetic phase with spin up in o-YMO and a ferromagnetic with spin down in LSMO and the interface. The geometries along with the magnetic structures are shown in Fig. 9.

We find that, in the range of typical Coulomb interaction ($U$ = 2–4 eV) for interface Mn atoms, the ground state of the heterostructure is a completely ferromagnetic phase with a magnetic configuration $3d^4\uparrow$ in o-YMO. The antiferromagnetic *E*-type in o-YMO and ferromagnetic in LSMO and the interface is the sum of the two bulk ground states. However, it is never the ground state of the heterostructure, although is very close in energy to the fully ferromagnetic solution. The *E*-type phase is the ground state in o-YMO bulk, and the energy difference between FM and AF is 3 meV per formula unit. However, the heterostructure stabilizes the ferromagnetic phase in o-YMO near the interface. Because of the different polarizations of the ferromagnetic phase of o-YMO, we should experimentally observe a reduction of polarization proportional to the number of layers that become ferromagnetic.

### 4.3. Large vertical shift

Zandalazini *et al.* (2011) found experimentally a vertical shift $m_{\rm shift}$ in the $YMnO_3/La_{0.7}Sr_{0.3}MnO_3$ heterostructure at 10 K and this vertical shift was attributed to the properties of the DAFF state. Instead, the nature of the large vertical shift might be found in the interdiffused ferromagnetic layer at the interface composed also by an unusual o-YMO ferromagnetic phase. The $m_{\rm shift}$ effect can be explained with a large coercivity of the ferromagnetic phase of o-YMO at the interface. To calculate the coercivity, we use the theory of single-domain reversal, which requires taking into account the magnetic field and the magnetocrystalline anisotropy energy. We suppose that all the anisotropies of the system originate from o-YMO, but in principle it is possible to have anisotropy also in orthorhombic LSMO near the interface or in the interface layer.

Considering a sample of 5 × 5 mm and a magnetization of 4 $\mu_B$ per Mn atom in o-YMO, we estimate that every fully ferromagnetic layer will give us a magnetization of 6.1 μemu. This value is very close to the value found for the LASMO sample at low temperature in Fig. 1(*c*). Therefore, we expect to have approximately one ferromagnetic layer in LASMO and two ferromagnetic layers in LBSMO at the interface. As there are two ferromagnetic layers, we cannot have the ferromagnetism just at the interface layer and we have at least one

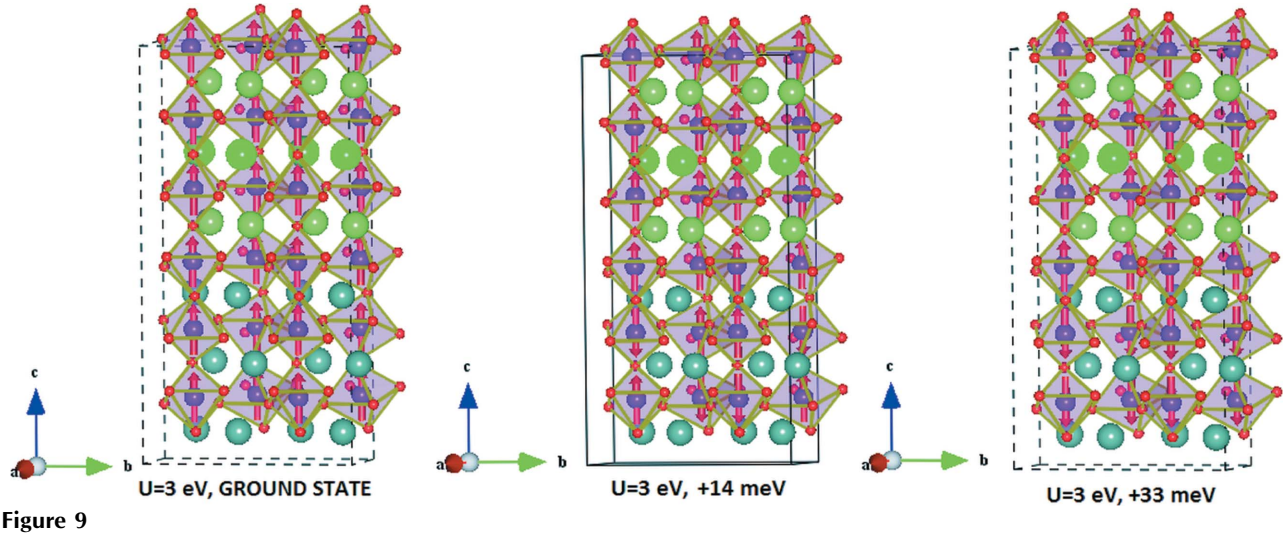


**Figure 9**
Some magnetic phases of the supercell at the interface. The $MnO_6$ octahedra are shown with red arrows that indicate the spins on Mn atoms. Only spin up and spin down are shown and not the direction of the spin that is in the *ab* plane. Y, La and Sr atoms are shown as dark-blue, dark-green and light-green balls. The first two layers in the bottom of the figure are o-YMO, after we have an interface layer, after there are the LSMO layers. The total energies with respect to the ground state are shown for $U$ = 3 eV for the interface Mn atoms. The left most picture is for the ground state that is completely ferromagnetic while the middle picture shows the sum of the two bulk ground states (ferromagnetic in LSMO and *E*-type in o-YMO) that is 14 meV higher in energy than the ground state. The right-most picture is for ferromagnetic LSMO and ferromagnetic interface, but with YMO that has opposite spin with respect to LSMO. The interface structures are shown for the ground state. The directions a and b are the same directions of the bulk o-YMO.

FM layer of o-YMO. This is the case for a sharp interface, but we expect that a large roughness at the interface may give us a large ferromagnetic interdiffused layer and hence a large $m_{shift}$. Therefore, one can safely conclude that the results obtained for a sharp interface are also valid for an interdiffused interface but with a larger effect.

**4.3.1. Magnetocrystalline anisotropy of bulk $YMnO_3$.** From the above discussion, one may come to the conclusion that a ferromagnetic o-YMO region may exist at the interface. Now we study the magnetic anisotropy energy of a hypothetical o-YMO ferromagnetic phase. As the magnetic field in the experiment is applied in the *ab* plane, we are interested in studying the magnetic anisotropy for the same situation. The formula for the anisotropy energy $E_A$ in the *ab* plane for this system is

$$E_A(\varphi) = K_2 \cos^2 \varphi, \tag{1}$$

where $\varphi$ is the angle between the *a* axis and the magnetization in the *ab* plane. Our calculated *ab initio* value of the magnetocrystalline anisotropy parameter for the ferromagnetic phase is $K_2 = 0.561$ meV per formula unit $= 160 \times 10^4$ J m$^{-3}$ $= 160 \times 10^5$ erg cm$^{-3}$. We find $K_2 > 0$, and therefore the easy axis is along the *b* axis for $\varphi = 90^\circ$, while the hard axis is along the *a* axis for $\varphi = 0^\circ$. The calculated values of $K_2$ are quite big compared to the values found in the literature for usual magnetic materials (Landolt–Börnstein, 1986; Cullity *et al.*, 2005; Daalderop *et al.*, 1990). Probably these large values come from the large ratio $b/a = 1.1114$ between the lattice parameters. We also calculate the energy with the spin along the *c*-axis direction, and we find that *c* axis is almost as hard as the *a* axis. Therefore we do not need to take into account the *c* axis in the anisotropy energy.

To simulate the hysteresis we need to take into account the interaction of the magnetic system with the external magnetic field. The effect of the magnetic field on the energy is represented by the Zeeman energy $E_H$, which is expressed as

$$E_H(\varphi) = -MH \cos(\varphi - \varphi_H), \tag{2}$$

where $\varphi_H$ is the direction of the external magnetic field $H$ and $\varphi - \varphi_H$ is the angle between the magnetic field and the magnetic moment $M$.

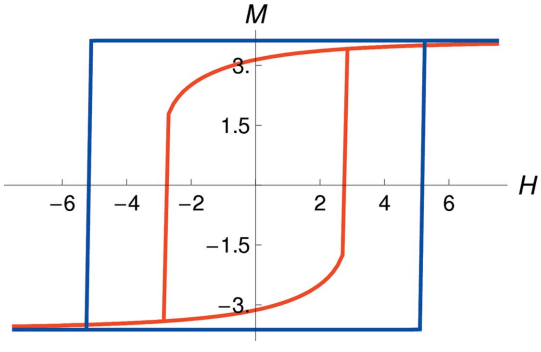


**Figure 10**
Hysteresis loop with $\varphi_H = 60^\circ$ (red line) and $\varphi_H = 90^\circ$ (blue line). Projection of magnetization along the $\varphi_H$ direction in $\mu_B$ per Mn atom. The unit of the magnetic field is Oe ($\times 10^4$).

Using the total energy $E_A + E_H$, we calculate the hysteresis for o-YMO. Other kinds of anisotropies are not taken into account, *e.g.* interface anisotropy and shape anisotropy. The magnitude of the total magnetic moment $\mathbf{M} = \mathbf{M}_{spin} + \mathbf{M}_{orbital}$ for the system is $M = 3.62\ \mu_B$ per Mn atom. We see from Fig. 10 that the coercive field $H_C$ is of the order of 2–5 $\times 10^4$ Oe, while in the experiment for the $YMnO_3/La_{0.7}Sr_{0.3}MnO_3$ heterostructure (Zandalazini *et al.*, 2011) the magnetic field was up to $0.5 \times 10^4$ Oe. The total energy is expressed as

$$E(\varphi) = K_2 \cos^2 \varphi - MH \cos(\varphi - \varphi_H), \tag{3}$$

and in particular we have that for $\varphi_H = 90^\circ$ there is only one stable solution for $H > H_C = 2K_2/M$, which is the coercive field in this limiting case. In our study, the coercivity is $5.4 \times 10^4$ Oe when the magnetic field is along the easy axis.

Finally, we want to comment on the magnetic anisotropy of the LSMO part. In LSMO (Suzuki *et al.*, 1998), a very small anisotropy parameter $K_2^{LSMO} = 0.18 \times 10^4$ J m$^{-3}$ was measured, where the easy axis is along the *c* axis and the hard axes are in the *ab* plane. In the present case of the heterostructure, we have in the LASMO sample a larger quantity of orthorhombic LSMO, while LBSMO is almost all pseudocubic. In the experiments, the coercive field $\mu_0 H_C \simeq 0.05 \times 10^4$ Oe is measured for LBSMO where there is a bulk pseudocubic LSMO, while a slightly larger $\mu_0 H_C \simeq 0.10 \times 10^4$ Oe was found in LASMO, owing to the orthorhombic LSMO (see Fig. 1). This happens because the orthorhombic LSMO is more anisotropic than the bulk pseudocubic one and has a higher coercive field. However, the values are very small compared to those for o-YMO, and therefore we can expect that the magnetic moment that produces the vertical shift does not come from orthorhombic LSMO.

## 5. Summary and conclusion

In summary, a large vertical shift ($m_{shift}$), unusual for an exchange bias system, was reported previously in LSMO/o-YMO bilayers. The vertical shifts were found to be inversely proportional to the horizontal shifts. In this paper, we have shown from depth-sensitive PNR measurements that the magnetization within an interdiffused layer (extending up to 100 Å) is responsible for the large $m_{shift}$ in LBSMO. This $m_{shift}$ decreases in LASMO with the thickness of the interdiffused layer. A change in temperature just above $T_N$ makes this magnetism decrease significantly. This indicates that the origin for the $m_{shift}$ is the o-YMO layer. More precisely, the magnitude of the $m_{shift}$ is related to the o-YMO-driven ferromagnetic LSMO/o-YMO interlayer, i.e on the characteristics of the ferromagnetic interdiffused layer.

By means of first-principles density functional theory, we determined the structural and electronic properties of $YMnO_3/La_{0.7}Sr_{0.3}MnO_3$ heterostructures in order to explain the origin of the vertical shift. We find that the interface stabilizes an unusual ferromagnetic phase of o-YMO, which is not found in the bulk. This FM phase is only present at the interface and has the same lattice constants of AF o-YMO. The ferromagnetic phase of o-YMO is a strongly anisotropic

ferromagnet with a large coercivity. If we compare this result with the experimental values of the vertical shift, we observe that the FM phase is composed of one to two interface layers of o-YMO. The $YMnO_3/La_{0.7}Sr_{0.3}MnO_3$ heterostructure is an interface between an isotropic ferromagnet (LSMO) and strongly anisotropic ferromagnet (o-YMO near the interface).

In conclusion, it was experimentally and theoretically shown that the magnetization within the interdiffused layer is responsible for the large vertical shift. The origin for the vertical shift is related to the o-YMO-driven ferromagnetic LSMO/o-YMO interface layer. Indeed, a relatively small magnetic field applied to the entire heterostructure can rotate the spin in LSMO, while the spin in o-YMO is constant because of the large coercivity. This constant magnetic moment in o-YMO is the vertical $m_{\rm shift}$.

Thus our study, in general, would instigate revisits of various other systems showing such vertical shifts.

BS and CA acknowledge financial support from Carl Tryggers Stiftelse (grant No. CTS 12:419). Also supercomputing time allocation from the Swedish National Infrastructure for Computing is greatly acknowledged.

## References


Barzola-Quiquia, J., Lessig, A., Ballestar, A., Zandalazini, C., Bridoux, G., Bern, F. & Esquinazi, P. (2012). *J. Phys. Condens. Matter*, **24**, 366006.

Cullity, B. D. & Graham, C. D. (2005). *Introduction to Magnetic Materials*. Hoboken: Wiley–IEEE Press.

Daalderop, G. H. O., Kelly, P. J. & Schuurmans, M. F. H. (1990). *Phys. Rev. B*, **41**, 11919.

Fitzsimmons, M. R., Dufour, C., Dumesnil, K., Dou, J. & Pechan, M. (2009). *Phys. Rev. B*, **79**, 144425.

Geshev, J. (2008). *J. Appl. Phys.* **104**, 023914.

Gibert, M., Zubko, P., Scherwitzl, R., Íñiguez, J. & Triscone, J.-M. (2012). *Nat. Mater.* **11**, 195–198.

Gruyters, M. & Schmitz, D. (2008). *Phys. Rev. Lett.* **100**, 077205.

He, C., Grutter, A. J., Gu, M., Browning, M. D., Yakamura, Y., Kirby, B. J., Borchers, J. A., Kim, J. W., Fitzsimmons, M. R., Zhai, X., Mehta, V. V., Wong, F. J. & Suzuki, Y. (2012). *Phys. Rev. Lett.* **109**, 197202.

Hong, J.-I., Leo, T., Smith, D. J. & Berkowitz, A. E. (2006). *Phys. Rev. Lett.* **96**, 117204.

Kresse, G. & Furthmüller, J. (1996). *Comput. Mat. Sci.* **6**, 15–50.

Kresse, G. & Joubert, D. (1999). *Phys. Rev. B*, **59**, 1758–1775.

Meiklejohn, W. H. & Bean, C. P. (1956). *Phys. Rev.* **102**, 1413.

Moutis, N., Christides, C., Panagiotopoulos, I. & Niarchos, D. (2001). *Phys. Rev. B*, **64**, 094429.

Munoz, A., Alonso, J. A., Casais, M. T., Martinez-Lope, M. J., Martinez, J. L. & Fernandez-Diaz, M. T. (2002). *J. Phys. Condens. Matter*, **14**, 3285.

Landolt-Börnstein (1986). *Magnetic Properties of Metals*, New Series, Group III, Vol. 19a, edited by H. P. J. Wijn. Heidelberg: Springer-Verlag.

Okuyama, D., Ishiwata, S., Takahashi, Y., Yamauchi, K., Picozzi, S., Sugimoto, K., Sakai, H., Takata, M., Shimano, R., Taguchi, Y., Arima, T. & Tokura, Y. (2011). *Phys. Rev. B*, **84**, 054440.

Ohldag, H., Scholl, A., Nolting, F., Arenholz, E., Maat, S., Young, A. T., Carey, M. & Stöhr, J. (2003). *Phys. Rev. Lett.* **91**, 017203.

Ohldag, H., Shi, H., Arenholz, E., Stöhr, J. & Lederman, D. (2006). *Phys. Rev. Lett.* **96**, 027203.

Panagiotopoulos, I., Christides, C., Pissas, M. & Niarchos, D. (1999). *Phys. Rev. B*, **60**, 485–491.

Passamani, E. C., Larica, C., Proveti, J. R., Marques, C., Takeuchi, A. Y. & Sanchez, F. H. (2006). *J. Magn. Magn. Mater.* **299**, 11–20.

Paul, A. (2012). *Pramana*, **78**, 1–58.

Paul, A., Paul, N., Jutimoosik, J., Yimnirun, R., Rujirawat, S., Höpfner, B., Lauermann, I., Lux-Steiner, M., Mattauch, S. & Böni, P. (2013). *Phys. Rev. B*, **87**, 014431.

Perdew, J. P., Burke, K. & Ernzerhof, M. (1996). *Phys. Rev. Lett.* **77**, 3865–3868.

Picozzi, S., Yamauchi, K. & Bihlmayer, G. & Blügel, S. (2006). *Phys. Rev. B*, **74**, 094402.

Suzuki, Y., Hwang, H. Y., Cheong, S. W., Siegrist, T., Van Dover, R. B., Asamitsu, A. & Tokura, Y. (1998). *J. Appl. Phys.* **83**, 7064–7066.

Tian, Y. F., Ding, J. F., Lin, W. N., Chen, Z. H., David, A., He, M., Hu, W. J., Chen, L. & Wu, T. (2013). *Sci. Rep.* **3**, 1094.

Ueda, K., Tabata, H. & Kawai, T. (1998). *Science*, **280**, 1064–1066.

Venta, J. de la, Erekhinsky, M., Wang, S., West, K. G., Morales, R. & Schuller, I. K. (2012). *Phys. Rev. B*, **85**, 134447.

Wu, S. M., Cybart, S. A., Yu, P., Rossell, M. D., Zhang, J. X., Ramesh, R. & Dynes, R. C. (2010). *Nat. Mater.* **9**, 756–761.

Zandalazini, C., Esquinazi, P., Bridoux, G., Barzola-Quiquia, J., Ohldag, H. & Arenholz, E. (2011). *J. Magn. Magn. Mater.* **323**, 2892–2898.

Ziese, M., Pippel, E., Nikulina, E., Arredondo, M. & Vrejoiu, I. (2011). *Nanotechnology*, **22**, 254025.

Ziese, M., Vrejoiu, I., Pippel, E., Esquinazi, P., Hesse, D., Etz, C., Henk, J., Ernst, A., Maznichenko, I. V., Hergert, W. & Mertig, I. (2010). *Phys. Rev. Lett.* **104**, 167203.